Evaluation of the $\pi\pi$-scattering amplitude in the σ-channel at finite density

D. Cabrera, E. Oset, and M. J. Vicente Vacas
Departamento de Física Teórica and IFIC, Centro Mixto Universidad de Valencia-CSIC, Ap. Correos 22085, E-46071 Valencia, Spain
(Received 11 March 2005; published 31 August 2005)

The $\pi\pi$ scattering amplitude in the σ-channel is studied at finite baryonic density in the framework of a chiral unitary approach which successfully reproduces the meson meson phase shifts and generates the f_0 and σ resonances in vacuum. We address here a new variety of mechanisms recently suggested to modify the $\pi\pi$ interaction in the medium, as well as the role of the s–wave selfenergy, in addition to the p–wave, in the dressing of the pion propagators.

DOI: 10.1103/PhysRevC.72.025207 PACS number(s): 13.75.Lb, 14.40.Aq, 14.40.Cs, 24.85.+p

I. INTRODUCTION

In the last years, several theoretical approaches have predicted strong medium effects on the pion pion interaction in the scalar isoscalar (σ) channel.

In Ref. [1], Hatsuda *et al*. studied the σ propagator in the linear σ model and found an enhanced and narrow spectral function near the 2π threshold caused by the partial restoration of the chiral symmetry, where m_σ would approach m_π. The same conclusions were reached using the nonlinear chiral Lagrangians in Ref. [2].

Similar results, with large enhancements in the $\pi\pi$ amplitude around the 2π threshold, have been found in a quite different approach by studying the s–wave, $I = 0$ $\pi\pi$ correlations in nuclear matter [3–6]. In these cases the modifications of the σ channel are induced by the strong p–wave coupling of the pions to the particle-hole (ph) and Δ-hole (Δh) nuclear excitations. It was pointed out in Refs. [7,8] that this attractive σ self-energy induced by the π renormalization in the nuclear medium could be complementary to additional s–wave renormalizations of the kind discussed in Refs. [1,2] calling for even larger effects.

On the experimental side, there are also several results showing strong medium effects in the σ channel at low invariant masses in the $A(\pi, 2\pi)$ [9–13] and $A(\gamma, 2\pi)$ [14] reactions. At the moment, the cleanest signal probably corresponds to the $A(\gamma, 2\pi^0)$ reaction, which shows large density effects that had been predicted in both shape and size in Ref. [15], using a model for the $\pi\pi$ final state interaction along the lines of the present work. Note, however, that a part of the spectrum modification could be due to quasielastic collisions of the pion [16].

Our aim in this paper is to study the $\pi\pi$ scattering in the scalar isoscalar (σ) channel at finite densities in the context of the model developed in Refs. [17–22]. These works, which provide an economical and successful description of a wide range of hadronic phenomenology, use as input the lowest orders of the Lagrangian of chiral perturbation theory (χPT) [23] and calculate meson meson scattering in a coupled channels unitary way. Some nuclear medium effects, namely the p–wave coupling of the pions to the particle hole (ph) and delta hole (Δh) excitations, were implemented in this framework in Refs. [6,24]. As in other approaches, large medium effects were found as reflected in the imaginary part of the $\pi\pi$ scattering amplitude which showed a clear shift of strength towards low energies as the density increases. Although this model was able to predict the size of the medium effects on the $(\gamma, 2\pi)$ reaction [15], it was pointed out that some probably large contributions related to nucleon tadpole diagrams [2] and some vertex corrections [30] were missing. In this work, we will include those pieces and analize its influence in the $\pi\pi$ scattering amplitude at finite nuclear densities.

In the next section we present, for the sake of completeness, a brief description of the model used for the $\pi\pi$ interaction both in vacuum and in a dense medium, which is already published elsewhere [6,24]. In Sec. III we consider further contributions to the $\pi\pi$ interaction in the nuclear medium, associated to higher order terms in the chiral Lagrangian than those included in Refs. [6,24], and some baryonic vertex corrections advocated in Ref. [30].

II. $\pi\pi$ INTERACTION

In this section we summarize the method of Ref. [22] for $\pi\pi$ interaction in vacuum and Refs. [6,24] for the nuclear medium effects. Additional information on this and related approaches for different spin isospin channels can be found in Refs. [19,20,22,25].

A. Vacuum

The basic idea is to solve a Bethe Salpeter (BS) equation, which guarantees unitarity, matching the low energy results to χPT predictions. We consider two coupled channels, $\pi\pi$ and $K\bar{K}$ and neglect the $\eta\eta$ channel which is not relevant at the low energies we are interested in.

The BS equation is given by

$$T = V + VGT. \tag{1}$$

Equation (1) is a matrix integral equation which involves the two mesons one loop divergent integral (see Fig. 1), where V and T appear off shell. However, for this channel both functions can be factorized on shell out of the integral. The remaining off shell part can be absorbed by a renormalization of the coupling constants as it was shown in Refs. [22,26]. Thus, the BS equation becomes purely algebraic and the VGT term, originally inside the loop integral, becomes then the product of V, G, and T, with V and T the on shell amplitudes

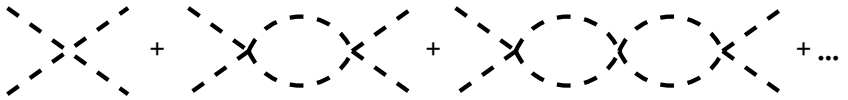

FIG. 1. Diagrammatic representation of the Bethe Salpeter equation.

independent of the integration variables, and G given by the expression

$$G_{ii}(P) = i \int \frac{d^4q}{(2\pi)^4} \frac{1}{q^2 - m_{1i}^2 + i\epsilon} \frac{1}{(P-q)^2 - m_{2i}^2 + i\epsilon}, \tag{2}$$

where P is the momentum of the meson meson system. This integral is regularized with a cutoff (Λ) adjusted to optimize the fit to the $\pi\pi$ phase shifts ($\Lambda = 1.03$ GeV).

The potential V appearing in the BS equation is taken from the lowest order chiral Lagrangian

$$\mathcal{L}_2 = \frac{1}{12f^2}\langle(\partial_\mu \Phi \Phi - \Phi \partial_\mu \Phi)^2 + M\Phi^4\rangle, \tag{3}$$

where the symbol $\langle\ \rangle$ indicates the trace in flavor space, f is the pion decay constant, and Φ, M are the pseudoscalar meson and mass SU(3) matrices. This model reproduces well phase shifts and inelasticities up to about 1.2 GeV. The σ and $f_0(980)$ resonances appear as poles of the scattering amplitude in $L = 0$, $I = 0$. The coupling of channels is essential to produce the $f_0(980)$ resonance, while the σ pole is little affected by the coupling of the pions to $K\bar{K}$ [22].

B. The nuclear medium

As we are mainly interested in the low energy region, which is not very sensitive to the kaon channels, we will only consider the nuclear medium effects on the pions. The main changes of the pion propagation in the nuclear medium come from the p–wave self-energy, produced basically by the coupling of pions to particle-hole (ph) and Delta-hole (Δh) excitations. For a pion of momentum q it is given by

$$\Pi(q) = \frac{\left(\frac{D+F}{2f}\right)^2 \vec{q}^{\,2} U(q)}{1 - \left(\frac{D+F}{2f}\right)^2 g' U(q)} \tag{4}$$

with $g' = 0.7$ the Landau-Migdal parameter, $U(q)$ the Lindhard function, and $(D + F) = 1.257$. The expressions for the Lindhard functions are taken from Ref. [27].

Thus, the in-medium BS equation will include the diagrams of Fig. 2 where the solid line bubbles represent the ph and Δh excitations.

In fact, as it was shown in [28], the contact terms with the ph (Δh) excitations of diagrams (b)–(d) cancel the off-shell contribution from the meson meson vertices in the term of Fig. 2(a). Hence, we just need to calculate the diagrams of the free type (Fig. 1) and those of Fig. 2(a) with the amplitudes factorized on shell. Therefore, at first order in the baryon density, we are left with simple meson propagator corrections which can be readily incorporated by changing the meson vacuum propagators by the in medium ones.

The $\pi\pi$ scattering amplitude obtained using this model exhibits a strong shift towards low energies. In Fig. 3, we show the imaginary part of this amplitude for several densities. Quite similar results have been found using different models [5] and it has been suggested that this accumulation of strength, close to the pion threshold, could reflect a shift of the σ pole which would approach the mass of the pion.

Other pion self-energy contributions related to $2ph$ excitations, and thus proportional to ρ^2, can be incorporated in the pion propagator. As we are most interested in the region of low energies we can take as estimation the corresponding piece of the optical potentials obtained from pionic atoms data, following the procedure of Ref. [6] and substituting in Eq. (4)

$$\left(\frac{D+F}{2f}\right)^2 U(q) \longrightarrow \left(\frac{D+F}{2f}\right)^2 U(q) - 4\pi C_0^* \rho^2 \tag{5}$$

with ρ the nuclear density and $C_0^* = (0.105 + i0.096) m_\pi^{-6}$. Its effects are small except at large densities as can be appreciated by comparing Fig. 3, with Fig. 7 of Ref. [6] where this piece is included.

III. FURTHER CONTRIBUTIONS

A. Higher order tadpole and related terms

The chiral Lagrangian generates tadpole terms that could contribute to the pion self-energy and also in the form of vertex corrections as in Fig. 4. At the lowest order these terms vanish in isospin symmetric nuclear matter [24]. However, at next order there are terms which provide some contribution. The complete structure of the higher order Lagrangian adapted to the πN system can be seen in Ref. [29]. The medium corrections associated to these new Lagrangian terms in the π nucleus interaction were studied in [40] and interpreted in terms of changes of the time and space components of f and changes of the pion mass in the medium. Further developments in this direction are done in Ref. [30].

The repercussion of these terms in $\pi\pi$ scattering in the nuclear medium has been considered in Ref. [2] and we follow here the same steps. We start from the second order πN Lagrangian relevant for the isoscalar sector

$$\mathcal{L}_{\pi N}^{(2)} = c_3 \bar{N}(u_\mu u^\mu) N + \left(c_2 - \frac{g_A^2}{8m_N}\right) \bar{N}(\mathrm{v}_\mu u^\mu)^2 N + c_1 \bar{N} N \mathrm{Tr}(U^\dagger \chi + \chi^\dagger U) + \cdots, \tag{6}$$

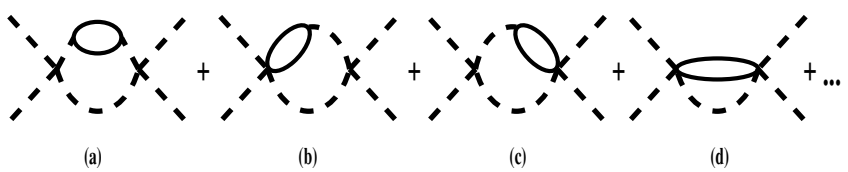

FIG. 2. Terms of the meson meson scattering amplitude accounting for ph and Δh excitation.

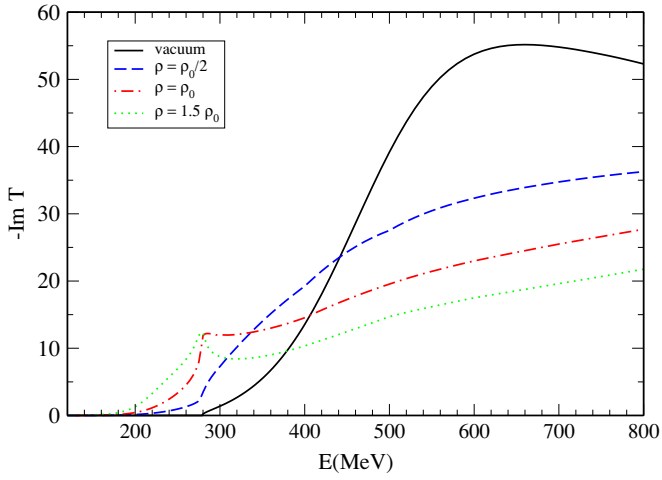

FIG. 3. (Color online) Imaginary part of the $\pi\pi$ scattering amplitude at several densities.

where $u_\mu = iu^\dagger\partial_\mu U u^\dagger$, with $U = u^2 = \exp(i\tau^a\phi^a/f)$ in the SU(2) formalism used there, v_μ is the four velocity of the nucleon, g_A the axial charge of the nucleon and $\chi = \mathrm{diag}(m_\pi^2, m_\pi^2)$. The pion nucleon amplitude obtained from the Lagrangian in Eq. (6) is

$$\begin{aligned} t_{\pi N} &= \frac{4c_1}{f^2}m_\pi^2 - \frac{2c_2}{f^2}(q^0)^2 - \frac{2c_3}{f^2}q^2 \\ &= \left[\frac{4c_1}{f^2}m_\pi^2 - \frac{2c_2}{f^2}\omega(q)^2 - \frac{2c_3}{f^2}m_\pi^2\right] - \frac{2c_2+2c_3}{f^2}(q^2 - m_\pi^2) \\ &= t_{\pi N}^{\mathrm{on}} + t_{\pi N}^{\mathrm{off}}, \end{aligned} \tag{7}$$

where in the last part of the equation we have separated what we call the on-shell part and the off-shell part of the amplitude [term with $(q^2 - m_\pi^2)$]. This s–wave πN interaction produces a modification of the pion propagator which we shall consider later in the solution of the Bethe-Salpeter equation in the medium.

In Refs. [2] and [40] the medium effects are recast at the mean field level in terms of a medium Lagrangian given by

$$\begin{aligned} \langle\mathcal{L}\rangle = &\left(\frac{f^2}{4} + \frac{c_3}{2}\rho\right)\mathrm{Tr}[\partial_\mu U\partial^\mu U^\dagger] + \left(\frac{c_2}{2} - \frac{g_A^2}{16m_N}\right)\rho \\ &\times \mathrm{Tr}[\partial_0 U\partial_0 U^\dagger] + \left(\frac{f^2}{4} + \frac{c_1}{2}\rho\right)\mathrm{Tr}(U^\dagger\chi + \chi^\dagger U). \end{aligned} \tag{8}$$

The different corrections to the $\pi\pi$ scattering amplitude coming from the $\partial_\mu U\partial^\mu U^\dagger$, $\partial_0 U\partial^0 U^\dagger$ terms and the mass term

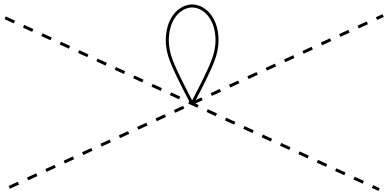

FIG. 4. Nucleon tadpole term correction to the $\pi\pi$ interaction.

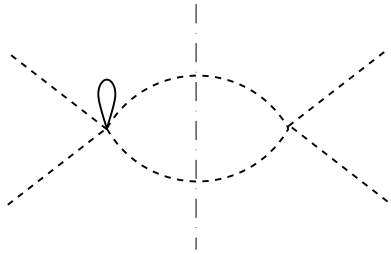

FIG. 5. $\pi\pi$ rescattering diagram with tadpole vertex correction showing the $\pi\pi$ cut.

in Eq. (8) (c_3, c_2, and c_1 terms) are given by

$$\begin{aligned} \delta t_{\pi\pi}^{(t)} = &-\frac{1}{f^2}\left\{\frac{2c_3}{f^2}\rho\left(s - \frac{4}{3}m_\pi^2\right) + \frac{2c_2}{f^2}\rho\left[s - \frac{1}{3}\sum_i \omega_i(q)^2\right]\right. \\ &\left. + \frac{c_1}{f^2}\rho\frac{5}{6}m_\pi^2\right\} + \frac{1}{f^2}\left\{\frac{2c_3}{f^2}\rho\frac{1}{3}\sum_i\left(q_i^2 - m_\pi^2\right) + \frac{2c_2}{f^2}\rho\right. \\ &\left.\times\frac{1}{3}\sum_i\left(q_i^2 - m_\pi^2\right)\right\}, \end{aligned} \tag{9}$$

where we have also separated the on-shell part from the off-shell part. These are the corrections coming from the many body tadpole diagram of Fig. 4, which are included in the ρ dependent terms of Eq. (8). Note that in the chiral unitary approach that we follow, the external legs are placed on shell ($q_i^2 = m_\pi^2$). This is the case even when the diagrams appear in loops, as in Fig. 5, since the underlying physics is the use of a dispersion relation using the N/D method [39,41] which determines the diagram contribution in terms of its imaginary part. In the case of Fig. 5 the cut corresponds to two free pions on shell, like in the vacuum. Hence, we shall use only the on shell part of the correction of Eq. (9).

As mentioned before, at the same time, when solving the Bethe-Salpeter equation, we have also to take into account the s–wave self-energy insertion from the Lagrangian of Eq. (6) in the pion propagators as depicted in Fig. 6. This is easily accounted for, at lowest order in ρ, adding to each pion propagator, D_π, the correction $D_\pi t_{\pi N}\rho D_\pi$. A technically simple way to account for that is to add to the scalar isoscalar

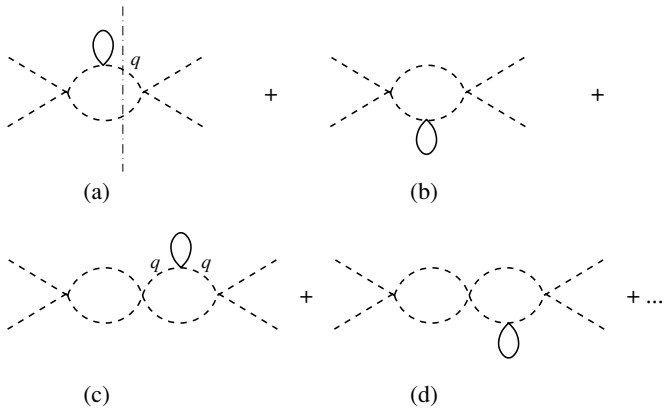

FIG. 6. Nucleon tadpole correction in the pion propagator.

$\pi\pi$ vertex from $\mathcal{L}_2$, $t_{\pi\pi}$, the correction

$$\delta t_{\pi\pi}^{(s)} = \left(t_{\pi N}^{\rm on} + t_{\pi N}^{\rm off}\right)\rho \frac{1}{q^2 - m_\pi^2} t_{\pi\pi} \tag{10}$$

for the two pion propagator lines to the left of the $\pi\pi$ vertex. Now the separation of the on-shell and off-shell parts of $t_{\pi N}$ is most useful since the pion propagator in Eq. (10) is canceled out by the $(q^2 - m_\pi^2)$ factor of the off-shell part of $t_{\pi N}$. Thus we have

$$\delta t_{\pi\pi}^{(s)} = t_{\pi N}^{\rm on}\rho \frac{1}{q^2 - m_\pi^2} t_{\pi\pi} - \frac{2c_2 + 2c_3}{f^2}\rho t_{\pi\pi}. \tag{11}$$

This means that with the Lagrangian used, on top of the corrections in the loops from the s–wave (on-shell) pion self-energy, we have an additional correction [second term of Eq. (11)] of the same topology as the tadpole term considered before. Considering the pion self-energy insertion in either of the two pion propagators, we obtain for this

$$\delta t_{\pi\pi}^{(\rm st)} = -\frac{4c_2 + 4c_3}{f^2}\rho t_{\pi\pi}. \tag{12}$$

Thus, we are left with the usual contribution in the pion loops of the ordinary on-shell s–wave pion self-energy, plus the tadpole correction of Eq. (9), plus the tadpole equivalent of Eq. (12).

There are still further contributions belonging to the same family. Indeed, the $t_{\pi\pi}$ amplitude in the scalar isoscalar channel,

$$t_{\pi\pi} = -\frac{1}{f^2}\left[s - \frac{m_\pi^2}{2} - \frac{1}{3}\sum_i \left(q_i^2 - m_\pi^2\right)\right], \tag{13}$$

is also split in on- and off-shell parts. In [6,42] it was shown that the off-shell pieces could be removed from the loop calculations for both the free pion case and the pion with a p–wave self-energy. However, the diagrams in Fig. 6(a) have one free pion and a pion with a s–wave medium self-energy insertion, hence the imaginary part of the two-pion loop is not the same as in the mentioned cases. It is again easy to take into account this correction and we have, from the s–wave self-energy insertions in the pion propagators

$$\delta t_{\pi\pi}^{(\rm so)} = t_{\pi N}\rho \frac{1}{q^2 - m_\pi^2}\frac{1}{3f^2}\left(q^2 - m_\pi^2\right) \equiv \frac{1}{3f^2} t_{\pi N}\rho \tag{14}$$

for each pion line. Next we separate the on-shell and off-shell parts of $t_{\pi N}$. For the on-shell part we get

$$\frac{1}{3f^2}\left[\frac{4c_1}{f^2}m_\pi^2 - \frac{2c_2}{f^2}\omega(q)^2 - \frac{2c_3}{f^2}m_\pi^2\right]\rho, \tag{15}$$

which compared at threshold to the free $t_{\pi\pi}$ amplitude, $t_{\pi\pi} = -\frac{1}{f^2}\frac{7}{2}m_\pi^2$, gives

$$\frac{\delta t_{\pi\pi}}{t_{\pi\pi}} \simeq \frac{1}{21 f^2}(8c_1 - 4c_2 - 4c_3)\rho, \tag{16}$$

which with respect to Eq. (12) gets a reduction of a factor 21, plus an extra reduction from the near on-shell cancellation of the isoscalar $t_{\pi N}$. Hence, this correction is negligible and we take advantage of this large reduction factor 21 to also neglect the part involving simultaneously the off-shell parts of $t_{\pi\pi}$ and $t_{\pi N}$.

TABLE I. c_i coefficients from Ref. [45].

Coefficient	Set I (GeV^{-1})	Set II (GeV^{-1})
c_1	−0.35	−0.32
c_2	−1.49	−1.59
c_3	0.93	1.15

In order to proceed we have to decide upon the c_i coefficients to be used. It is well known that the Lagrangian of Eq. (6) leads to a part of p–wave pion self-energy [43], but we are explicitly taking a p–wave self-energy insertion accounting for ph and Δh excitations. There is a work which uses the same Lagrangian of Eq. (6), and in addition takes into account explicitly the Δ degrees of freedom [44]. Thus, we stick to the values of the c_i coefficients obtained there from two fits, with and without using the σ term as a constraint, shown in Table I. For comparison, the values of the coefficients c_i without including the Δ are of the order of $c_1 = -1.53\,\mathrm{GeV}^{-1}$, $c_2 = 3.22\,\mathrm{GeV}^{-1}$ and $c_3 = -6.20\,\mathrm{GeV}^{-1}$ [45].

As stressed in Ref. [45] the values of the coefficient c_i with the explicit contribution of the Δ are of natural order, while those obtained without its consideration are too large and a source of problems in chiral perturbative calculations [46]. But in our case, as pointed above, the choice is mandatory.

We can estimate the size of the correction of Eq. (9) at pion threshold, and taking advantage of the reduction factor 1/3 in the term $\frac{1}{3}\omega_i^2(q)$ in front of $s \simeq 4m_\pi^2$, we approximate $\omega_i(q) \simeq m_\pi$. So we get

$$\frac{\delta t_{\pi\pi}}{t_{\pi\pi}} = \frac{32}{21 f^2}(c_2 + c_3)\rho + \frac{10}{21 f^2}c_1\rho, \tag{17}$$

which for the two sets of parameters of Table I gives

$$\begin{aligned}\frac{\delta t_{\pi\pi}}{t_{\pi\pi}} &= -0.154\rho/\rho_0 \text{ (set I)} \\ &= -0.124\rho/\rho_0 \text{ (set II)}.\end{aligned} \tag{18}$$

Let us note that the correction is negative, reducing effectively the strength of the $\pi\pi \to \pi\pi$ vertex in the medium. Note that should we have used the values of c_i without explicit Δ we would obtain a value for the ratio of Eq. (17) of $-0.80\rho/\rho_0$, certainly too large, but also negative.

Next we consider the contribution from Eq. (12). This correction has opposite sign to the former one. When adding the two corrections we find, again taking the threshold for comparison,

$$\frac{\delta t_{\pi\pi}}{t_{\pi\pi}} = -\frac{52}{21 f^2}(c_2 + c_3)\rho + \frac{10}{21 f^2}c_1\rho, \tag{19}$$

which for the two sets of values of Table I gives

$$\begin{aligned}\frac{\delta t_{\pi\pi}}{t_{\pi\pi}} &= 0.18\rho/\rho_0 \text{ (set I)} \\ &= 0.14\rho/\rho_0 \text{ (set II)}.\end{aligned} \tag{20}$$

We can see that the sign of the correction is now reversed and, altogether, we find now an effective increase of the $\pi\pi$ vertex in the medium by a moderate amount.

Apart from the vertex corrections, we need to include the effect of the on-shell s–wave pion self-energy in the pion

propagators in the loops, produced by the nucleon tadpole diagram. Since we have a broad range of pion energies in the loop, we have used the $t\rho$ approximation for the s–wave pion self-energy and the amplitude t has been taken from the experimental fit to data [37]. This is a more realistic approach than to take the expression from the model used here which gives a too large s–wave scattering amplitude at high energies, and in any case produces a minor effect.

The considered corrections are included in the $\pi\pi$ amplitude by modifying the kernel of the BS equation with the on-shell part of Eqs. (9) and (12), namely

$$T = \frac{V + \delta t_{\pi\pi}^{(t)\,\mathrm{on}}}{1 - (V + \delta t_{\pi\pi}^{(t)\,\mathrm{on}} + \delta t_{\pi\pi}^{(\mathrm{st})})\, G}, \tag{21}$$

and modifying the pion propagators in the calculation of the two-pion loop function, G, as explained in Sec. III A.

B. Vertex corrections from baryonic loops

In the previous sections we have considered relevant medium effects, according to the pion nucleus phenomenology, which describe correctly the pion in the medium in a wide range of energies. These mechanisms lead to s– and p–wave pion self-energies in the propagators of the BS equation and some associated vertex corrections. In Ref. [30], other vertex corrections to the $\pi\pi$ amplitude which could provide some effect at low energies, where the leading p–wave pion self-energy is not so strong, were studied.

The mechanisms considered in Ref. [30] relevant for $\pi\pi$ s–wave scattering, modifying the kernel of the Bethe-Salpeter equation in the $\pi\pi$ interaction, are shown in Fig. 7. The $\pi\pi$ isoscalar contribution in the s channel for the ph excitation in the t channel in Fig. 7(a) is given, with the unitary normalization, by

$$-it = -\left(\frac{1}{4f^2}\right)^2 (p_1^0 + k_1^0)(p_2^0 + k_2^0) U(q) = \tilde{t} U(q), \tag{22}$$

where $U(q)$ is the ordinary Lindhard function for ph excitation, including a factor 2 of isospin (see Appendix of [27]). The second equation in Eq. (22) defines $\tilde{t}$. We have neglected the isoscalar πN amplitude in Eq. (22) since it is very small compared with the isovector one [31].

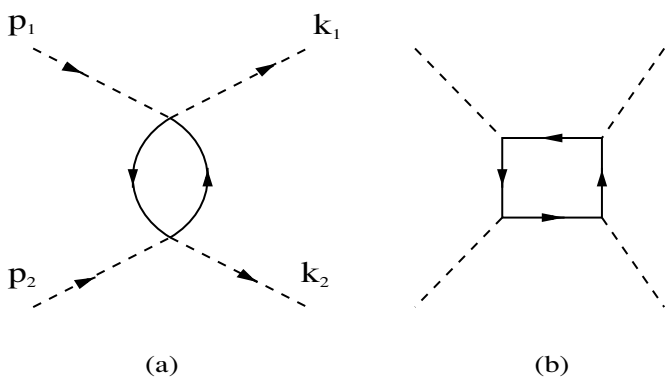

FIG. 7. (a) ph bubble exchange in the t channel; (b) Box diagram.

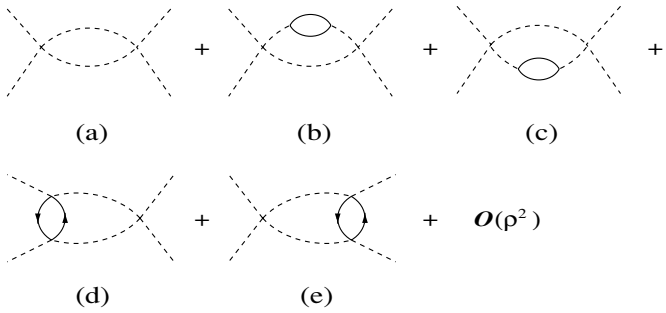

FIG. 8. Loop contributions to the Bethe-Salpeter equation at first order in the nuclear density, including the t–channel ph excitation.

The magnitude of t was shown in Ref. [30] to be comparable to the s–wave V of the lowest order chiral Lagrangian at densities of the order of the nuclear density. Yet, there are some observations to be made: First, at pion threshold the diagram of Fig. 7(a) is proportional to $U(q^0 = 0, \vec{q} = \vec{0})$. This quantity is evaluated in Ref. [30] using the ordinary limit of the Lindhard function at $q^0 = 0$ and $|\vec{q}| \to 0$, which is finite and larger in size than for any finite value of $|\vec{q}|$. This limit is however quite different from the value of the response function at $\vec{q} = \vec{0}$ in finite nuclei which is strictly zero, as already noted in [30,32,33].

We take into account the fact that the isovector πN amplitude reflects the exchange of a ρ in the t channel [34] and multiply $(4f^2)^{-2}$ by a factor reflecting the two ρ propagators, $F(q) = [M_\rho^2/(M_\rho^2 + \vec{q}^{\,2})]^2$.

In order to estimate the importance of this contribution as compared to the p–wave pion self-energy insertions, we have evaluated the diagrams (a)–(e) in Fig. 8. Details of the calculation are given in Appendix B. The results are shown in Fig. 9 for the imaginary part of the resulting amplitude. We find that the contribution of diagrams (d),(e) is smaller than the changes produced by the insertion of the p–wave pion self-energy in the pion propagators. Similar results are found for the real part of the amplitude.

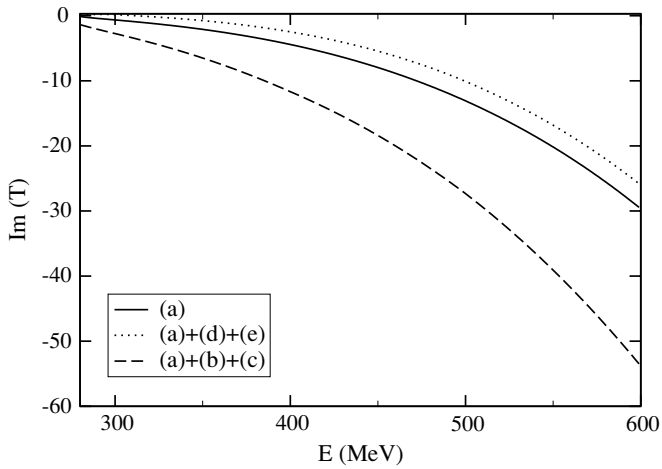

FIG. 9. Imaginary part of the $\pi\pi$ amplitude from the terms in Fig. 8, as indicated in the legend. The calculation for the dashed and dotted lines is done for $\rho = \rho_0/2$.

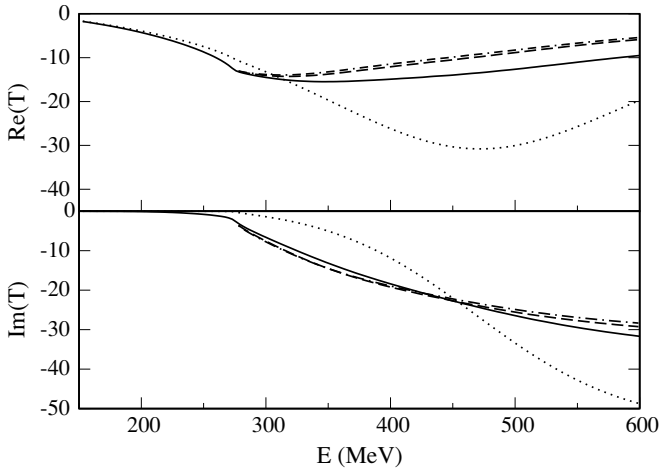

FIG. 10. Real and imaginary parts of T, as obtained in Eq. (21), for the two sets of parameters in Table I (set I, dash-dotted line; set II, dashed line) and $\rho = \rho_0/2$. The solid line corresponds to the result of the model in Sec. II A and the dotted line is the result in vacuum.

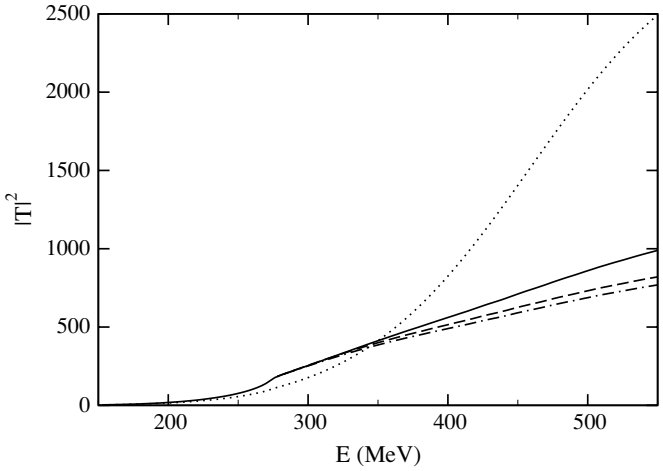

FIG. 11. Squared modulus of T. Lines as in Fig. 10.

The consideration of this mechanism in the BS equation proceeds by adding the tree level term and modifying the kernel in the loop terms with an effective potential δV defined as

$$\frac{\delta V(s,\rho)}{V} = \frac{\mathcal{F}(s,\rho)}{VGV}, \tag{23}$$

where $\mathcal{F}(s,\rho)$ is the amplitude corresponding to diagram (b) and VGV gives the amplitude of diagram (a) in Fig. 8. In this sense, by substituting V by $V + \delta V$ in the $\pi\pi$ vertex, the loop function of diagram in Fig. 8(a) would account correctly for all the diagrams (a)–(e) at the first order in the nuclear density.

One of the reasons for the small size of this contribution is that the Lindhard function behaves roughly as q^{-2} for large values of q and we should expect a large cancellation of this piece in the loops. This would be in contrast with the *ph* excitations leading to the p–wave π self-energy in Fig. 8(b), 8(c), since there one has the combination $\vec{q}^{\,2}U(q)$ and *a priori* this type of *ph* excitation should be more important, as it is indeed the case. Thus, the t-channel *ph* exchange mechanism leads to a sizable correction to the tree level $\pi\pi$ scattering amplitude and a small vertex correction in the calculation of the loops appearing in the unitarization procedure.[1]

Next we consider the box diagram of Fig. 7(b). This term was found to be smaller in strength than the *ph* exchange in Ref. [30], particularly at small energies, where the p–wave character of the vertices made the contribution negligible. The consideration of this mechanism at the pion loop level, necessary to include it in the BS equation, makes its contribution small since, apart from the reduction of the box diagram for large values of q, there is a further cancellation of terms as we show in Appendix C. Similar analytic treatments are done in Refs. [35,36]. For all these reasons this contribution should be even smaller than the one previously evaluated and one can safely neglect it for practical purposes.

IV. RESULTS

We solve the BS equation including the corrections discussed in Sec. III A, as they appear in Eq. (21). The results are shown in Fig. 10. The new terms considered modify little the results from Ref. [6]. In comparison, the imaginary part of the $\pi\pi$ amplitude exhibits a small increase of strength at low invariant energies whereas the real part decreases over all the calculated range of energies. Altogether, the basic effect of the nuclear medium, as found in Ref. [6], is a strong depletion of the interaction at energies around 500 MeV, where the vacuum σ pole is found, and some accumulation of strength close to the 2π threshold, as it can be seen in Fig. 11, where the squared modulus of the amplitude is depicted.

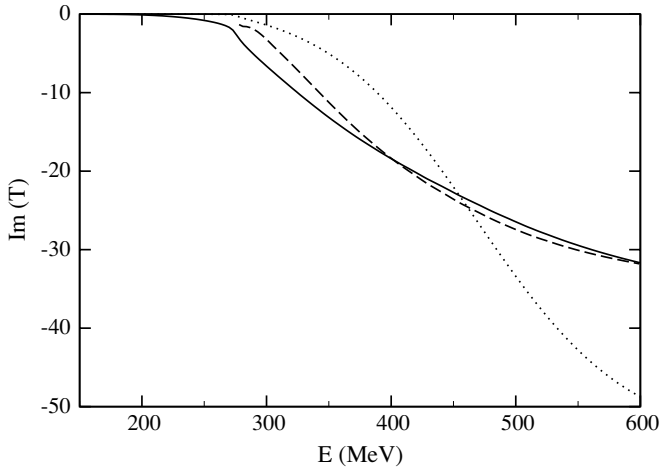

FIG. 12. Imaginary part of T including the mechanism described in Sec. III B at $\rho = \rho_0/2$ (dashed line). The solid line corresponds to the result of the model in Sec. II B and the dotted line is the result in vacuum.

[1]This mechanism would play an even smaller role in the position of the σ pole [47], which is determined by the vanishing of the denominator of the BS solution, where the tree level term does not appear.

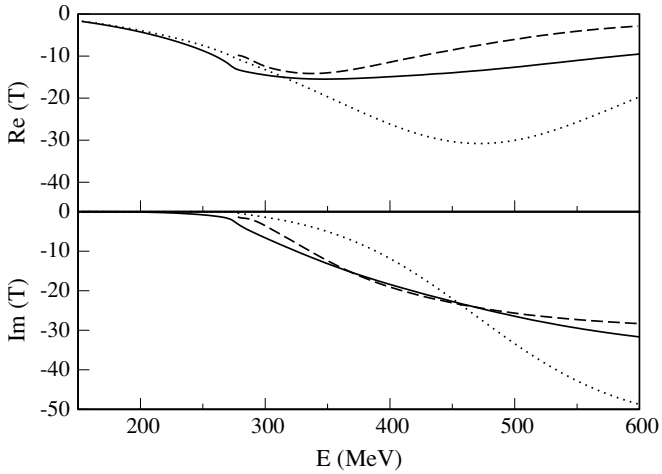

FIG. 13. Real and imaginary parts of T including the mechanisms described in Secs. III A and III B at $\rho = \rho_0/2$, using set I (dashed line). The solid line corresponds to the result of the model in Sec. II B and the dotted line is the result in vacuum.

The contribution of the terms discussed in Sec. III B is shown in Fig. 12 for the imaginary part of the $\pi\pi$ amplitude. We find a strong reduction of the amplitude at energies close to the 2π threshold, basically produced by the repulsive tree level term in Fig. 7(a). At these energies the amplitude stays closer to the vacuum case. A similar reduction of the nuclear medium effects as compared to the results of Ref. [6] is found in the real part of the amplitude.

Finally, we have included together the contributions of the tadpole terms, Sec. III A, and the t-channel ph exchange, Sec. III B, in the BS equation, and the results are depicted in Fig. 13 for the real and imaginary parts of the $\pi\pi$ amplitude. We observe, compared to the model of Ref. [6] in which the basic medium effect is due to the p–wave pion self-energy, a considerable reduction of strength close to the two pion threshold. The global effect in both calculations is still a sizable depletion of the interaction at higher energies and a certain accumulation of strength below the σ pole position in vacuum which, as suggested in Ref. [47], could be reflecting a change in the σ pole position to lower energies as a function of the nuclear density.

V. CONCLUSIONS

In summary, we have considered in this work the contribution of some new terms to the $\pi\pi$ interaction in the scalar isoscalar channel at finite densities, starting from a previous work [6,24] in which only medium effects associated to the p–wave pion self-energy had been accounted for.

Tadpole insertions, sometimes advocated as a possible source of a large attraction, have been shown to affect little the $\pi\pi$ amplitude once the Bethe-Salpeter equation is solved. This is partly due to certain cancellations which take place between vertices and internal pion propagator insertions.

We have also taken into account new terms in the driving kernel of the Bethe-Salpeter equation, which have been found to be important in a study based on a chiral power counting in the many body problem. We could see that these new terms, although large at tree level, when appearing inside loops were not as important as one could guess from their comparison with the lowest order chiral $\pi\pi$ amplitude in the case that all pions are on shell. As a consequence, their consideration barely changed the results for the $\pi\pi$ interaction in the medium.

Altogether, the final results are quite similar to those obtained previously in Refs. [6,24], namely, a strong reduction of the interaction at energies around 400 MeV and beyond, and some increase of strength around the 2π threshold. This confirms the leading role of the strong p–wave pion self-energy in the medium modification of the $\pi\pi$ interaction in the scalar isoscalar channel. These results are also satisfactory because a prediction on the $(\gamma, 2\pi)$ reaction in nuclei [15] based on the previous calculation [6,24] of the two-pion final state interaction has been later confirmed by experimental data [14]. The much larger medium effects obtained at threshold energies in other approaches are incompatible with the observed effect in the $(\gamma, 2\pi)$ reaction.

ACKNOWLEDGMENTS

This work was partly supported by DGICYT Contract No. BFM2003-00856. D.C. acknowledges financial support from MEC.

APPENDIX A

We quote in this section the Lindhard function, with an energy gap Δ, separated into the direct and crossed contributions, $U = U_d + U_c$. From Ref. [33] we have

$$U_d(q^0, \vec{q}, \Delta; \rho) = 4 \int \frac{d^3p}{(2\pi)^3} \frac{n(\vec{p})[1 - n(\vec{p} + \vec{q})]}{q^0 + \varepsilon(\vec{p}) - \varepsilon(\vec{p} + \vec{q}) - \Delta + i\epsilon} \tag{A1}$$

and $U_c(q^0, \vec{q}, \Delta; \rho) \equiv U_d(-q^0, \vec{q}, \Delta; \rho)$. In the following we shall use the definitions

$$\begin{aligned} x &= \frac{q}{k_F}, \qquad \nu = \frac{2Mq^0}{k_F^2}, \\ \delta &= \frac{2M\Delta}{k_F^2}, \quad \rho = \frac{2}{3\pi^2} k_F^3 \end{aligned} \tag{A2}$$

with M the mass of the nucleon, k_F the Fermi momentum, and $q \equiv |\vec{q}|$. Once the integration in Eq. (A1) is done, the real part of U_d reads, for $x \leqslant 2$,

$$\begin{aligned} &\mathrm{Re}\, U_d(q^0, \vec{q}, \Delta; \rho) \\ &= -\frac{2Mk_F}{\pi^2} \frac{1}{2x} \left\{ \frac{x}{2} - \frac{\nu - \delta}{4} + \frac{\nu - \delta}{2} \ln \left| \frac{\nu - \delta + x^2 - 2x}{\nu - \delta} \right| \right. \\ &\left. + \frac{1}{2} \left[1 - \frac{1}{4} \left(\frac{\nu - \delta}{x} - x \right)^2 \right] \ln \left| \frac{\nu - \delta - x^2 - 2x}{\nu - \delta + x^2 - 2x} \right| \right\} \end{aligned} \tag{A3}$$

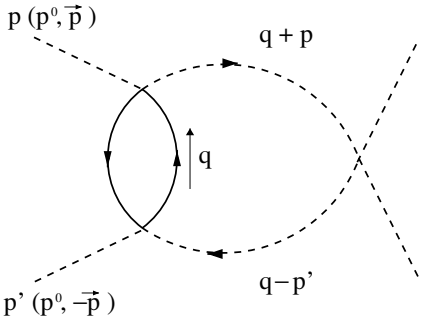

FIG. 14. Loop contribution of the *ph* exchange in the *t* channel.

and, for $x > 2$,

$$\mathrm{Re}\, U_d(q^0,\vec{q},\Delta;\rho) = -\frac{2Mk_F}{\pi^2}\frac{1}{2x}\left\{\frac{-\nu+\delta+x^2}{2x}+\frac{1}{2}\left[1-\frac{1}{4}\left(\frac{\nu-\delta}{x}-x\right)^2\right]\times\ln\left|\frac{\nu-\delta-x^2-2x}{\nu-\delta-x^2+2x}\right|\right\}. \quad \text{(A4)}$$

The imaginary part of U_d is given by $\mathrm{Im}\, U_d(q^0,\vec{q},\Delta;\rho) = \mathrm{Im}\,\tilde{U}(q^0-\Delta,\vec{q};\rho)\Theta(q^0-\Delta)$, with

$$\mathrm{Im}\,\tilde{U}(q^0,\vec{q};\rho) = -\frac{3}{4}\pi\rho\frac{M}{qk_F}[(1-z^2)\Theta(1-|z|) - (1-z'^2)\Theta(1-|z'|)]\frac{q^0}{|q^0|}, \quad \text{(A5)}$$

where Θ is the Heaviside step function and the z, z' variables are defined as

$$z = \frac{M}{qk_F}\left[q^0-\frac{q^2}{2M}\right], \quad z' = \frac{M}{qk_F}\left[-q^0-\frac{q^2}{2M}\right]. \quad \text{(A6)}$$

APPENDIX B

The amplitude corresponding to the diagram in Fig. 14 is given by

$$-iT = \int\frac{d^4q}{(2\pi)^4}(-i\tilde{t})\frac{i}{(q+p)^2-m_\pi^2+i\epsilon}\times\frac{i}{(q-p')^2-m_\pi^2+i\epsilon}[-iV(s)]iU(q). \quad \text{(B1)}$$

In order to perform the integral it is most useful to separate $U(q)$ into the direct and crossed parts, $U(q) = U_d(q) + U_c(q)$, given their different analytical structure.

In Fig. 15 we depict the pole and cut structure for the different terms and the path followed for the integration in the complex plane. The poles are located at

$$q^0 = -p^0+\omega(\vec{p}+\vec{q})-i\epsilon, \quad q^0 = -p^0-\omega(\vec{p}+\vec{q})+i\epsilon,$$
$$q^0 = p^0+\omega(\vec{p}+\vec{q})-i\epsilon, \quad q^0 = p^0-\omega(\vec{p}+\vec{q})+i\epsilon. \quad \text{(B2)}$$

The integration over the q^0 variable is done by closing the contour in the complex plane in the upper half plane for the U_d part and in the lower half plane for the U_c part.

The result of the integration is

$$T = -\left(\frac{1}{4f^2}\right)^2(2p^0)^2V(s)\int\frac{d^3q}{(2\pi)^3}\frac{1}{4\omega^2}\left\{\frac{U_c(p^0+\omega,\vec{q})}{p^0+\omega} - \frac{U_d(p^0-\omega,\vec{q})}{p^0-\omega+i\epsilon}+\frac{U_d(p^0-\omega,\vec{q})-U_c(p^0+\omega,\vec{q})}{p^0}\right\}\times\left(\frac{M_\rho^2}{M_\rho^2+\vec{q}^{\,2}}\right)^2, \quad \text{(B3)}$$

where $\omega \equiv \omega(\vec{p}+\vec{q})$ and we have explicitly written the ρ meson exchange form factor arising from each $\pi\pi NN$ vertex.

Let us note that we have factorized the $\pi N \to \pi N$ vertex on shell. This is done in analogy to what is done in Ref. [38] where one shows that the off shell part can be cast into a renormalization of the lowest order diagram (no meson loop in this case). An alternative justification using dispersion relations, which require only the on shell information, is given in Ref. [39].

APPENDIX C

We evaluate the loop function of Fig. 16 containing the box diagram of Fig. 7(b) plus all the different time orderings, which we can see in Fig. 17. In all the diagrams the internal nucleon lines are particle lines. This means we are taking only the terms of order ρ, which are obtained when the external lines are folded to give a single hole line in Fig. 17.

Diagrams (a), (b). For diagrams (a), (b) in Fig. 17 for $\vec{P} = \vec{p}_1 + \vec{p}_2 = \vec{0}$ the intermediate nucleon line after the two pion vertices has the same momentum as the hole line (belonging to the Fermi sea) and hence they both vanish.

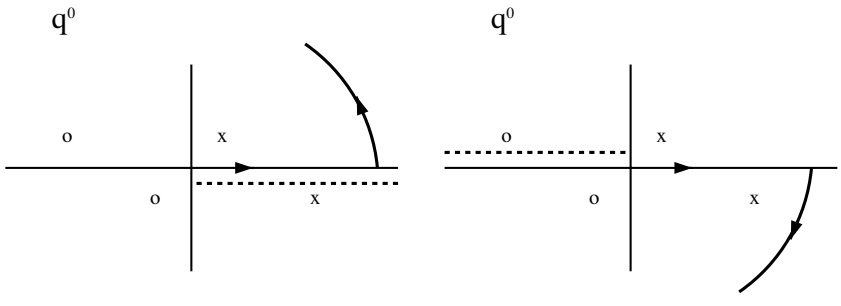

FIG. 15. Analytical structure of the integrand in Eq. (B1). The poles of the pion propagators are represented by "*x*" and "*o*" symbols, and the dotted lines correspond to the analytical cuts of the Lindhard function. The arrows indicate the circuit used for the integration of each term.

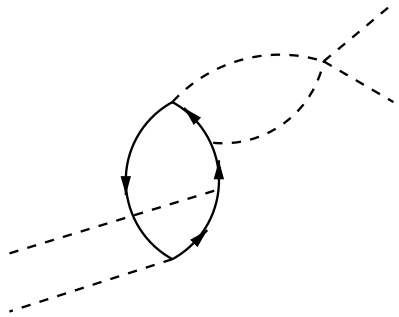

FIG. 16. Box diagram with two of the pions as a part of a loop.

Next we observe some strong cancellations in the other diagrams. The set of the two meson propagators, which is common to all of them, can be written as

$$\frac{1}{2P^0\omega}\left\{\frac{1}{q^0-\omega+i\epsilon}\ \frac{1}{q^0+P^0+\omega-i\epsilon} - \frac{1}{q^0+\omega-i\epsilon}\ \frac{1}{q^0+P^0-\omega+i\epsilon}\right\}, \quad \text{(C1)}$$

with $\omega=\omega(\vec{q})$.

Diagrams (c). The diagram (c) contains three nucleon propagators. By making a heavy baryon approximation and neglecting the kinetic energy of the nucleons we find for the product

$$\frac{1}{-p_1^0}\ \frac{1}{q^0+p_2^0+i\epsilon}\ \frac{1}{q^0+i\epsilon}. \quad \text{(C2)}$$

Hence, multiplying this by the pion propagators and closing the contour on the upper half plane to perform the q^0 integration, we find that the integral is

$$A\frac{1}{p_1^0}\left\{-\frac{1}{p_1^0+\omega}\ \frac{1}{P^0+\omega}+\frac{1}{\omega}\ \frac{1}{p_2^0-\omega+i\epsilon}\right\}. \quad \text{(C3)}$$

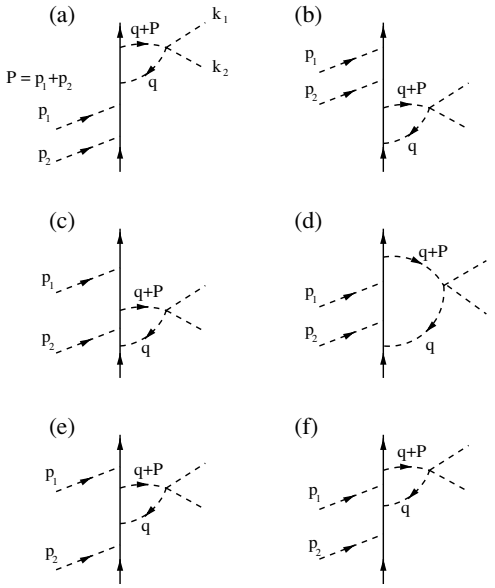

FIG. 17. Set of different time orderings of diagram in Fig. 16. The initial and final nucleon lines correspond to a hole propagator.

There, the first term, which comes from the negative energy components of the mesons, is small and has no imaginary part. The second term can lead to an imaginary part and a more sizable real part from the principal value.

Diagram (e). The set of nucleon propagators in the heavy baryon approximation is now

$$\frac{1}{p_2^0}\ \frac{1}{p_2^0+q^0+i\epsilon}\ \frac{1}{-p_1^0} \quad \text{(C4)}$$

and hence by closing the contour in the upper half of the complex q^0 plane we find for the q^0 integration

$$A\frac{1}{p_1^0}\left\{\frac{1}{p_2^0}\ \frac{1}{p_1^0+\omega}-\frac{1}{p_2^0}\ \frac{1}{p_2^0-\omega+i\epsilon}\right\}, \quad \text{(C5)}$$

with the same A as in Eq. (C3). The first term is again small, coming from the negative energy components of the pions, and has opposite sign to the first term from diagram (c). The second term above is the same but with opposite sign to the second term of diagram (c) at $\omega=p_2^0$, which is the singular point. Hence there are strong cancellations in the principal part of the integral and the imaginary part from this source vanishes.

Diagram (d). Repeating the same arguments as above we find now

$$-A\frac{1}{\omega}\left\{\frac{1}{p_1^0+\omega}\ \frac{1}{P^0+\omega}+\frac{1}{P^0-\omega+i\epsilon}\ \frac{1}{p_2^0-\omega+i\epsilon}\right\}. \quad \text{(C6)}$$

Diagram (f). For this diagram we find

$$A\frac{1}{p_1^0}\left\{\frac{1}{\omega}\frac{1}{p_2^0+\omega}-\frac{1}{P^0-\omega+i\epsilon}\frac{1}{p_1^0-\omega+i\epsilon}\right\}. \quad \text{(C7)}$$

Once again the first two terms from (d), (f), coming from the negative energy part of the pion propagators, give a small contribution and partly cancel, and the second terms which provide an imaginary part and a larger real part from the principal value, also show cancellations. Indeed for $p_1^0=p_2^0=\omega$ the imaginary parts corresponding to the poles $p_1^0=p_2^0=\omega$ cancel and the real parts from the principal value would also largely cancel. At the $P^0=\omega$ pole the cancellation would only be partial.

We thus see that when considering all the time orderings for the coupling of the two pions and the loop with the two pion propagators there are large cancellations of terms. In addition we have the $(p_i/M)^2$ factor of the p–wave couplings for the initial pions, which make this contribution small at small momenta of the pions. We have looked at strong cancellations of terms in the heavy baryon approximation, which holds for small values of momenta. At large momenta we must note that we have two extra nucleon propagators which bring two extra powers of q in the denominator, with respect to the ordinary Lindhard function. This makes up for the two extra p–wave vertices, and hence we have a similar behavior altogether as the one of Fig. 14 which lead to small contributions when evaluated into the loop. All these elements discussed above would render this piece far smaller than the ones of Fig. 8(d), 8(e) and, given the smallness of the effects found there, this can also be neglected.

[1] T. Hatsuda, T. Kunihiro, and H. Shimizu, Phys. Rev. Lett. **82**, 2840 (1999).
[2] D. Jido, T. Hatsuda, and T. Kunihiro, Phys. Rev. D **63**, 011901(R) (2000).
[3] P. Schuck, W. Norenberg, and G. Chanfray, Z. Phys. A **330**, 119 (1988).
[4] R. Rapp, J. W. Durso, and J. Wambach, Nucl. Phys. **A596**, 436 (1996).
[5] Z. Aouissat, R. Rapp, G. Chanfray, P. Schuck, and J. Wambach, Nucl. Phys. **A581**, 471 (1995).
[6] H. C. Chiang, E. Oset, and M. J. Vicente-Vacas, Nucl. Phys. **A644**, 77 (1998).
[7] Z. Aouissat, G. Chanfray, P. Schuck, and J. Wambach, Phys. Rev. C **61**, 012202(R) (1999).
[8] D. Davesne, Y. J. Zhang, and G. Chanfray, Phys. Rev. C **62**, 024604 (2000).
[9] F. Bonutti *et al*. (CHAOS Collaboration), Phys. Rev. Lett. **77**, 603 (1996).
[10] F. Bonutti *et al*. (CHAOS Collaboration), Nucl. Phys. **A638**, 729 (1998).
[11] P. Camerini, N. Grion, R. Rui, and D. Vetterli, Nucl. Phys. **A552**, 451 (1993) [Erratum-*ibid*. **A572**, 791 (1993)].
[12] F. Bonutti *et al*. (CHAOS Collaboration), Phys. Rev. C **60**, 018201 (1999).
[13] A. Starostin *et al*. (Crystal Ball Collaboration), Phys. Rev. Lett. **85**, 5539 (2000).
[14] J. G. Messchendorp *et al*., Phys. Rev. Lett. **89**, 222302 (2002).
[15] L. Roca, E. Oset, and M. J. Vicente Vacas, Phys. Lett. **B541**, 77 (2002).
[16] P. Muhlich, L. Alvarez-Ruso, O. Buss, and U. Mosel, Phys. Lett. **B595**, 216 (2004).
[17] A. Dobado, M. J. Herrero, and T. N. Truong, Phys. Lett. **B235**, 134 (1990).
[18] A. Dobado and J. R. Pelaez, Phys. Rev. D **47**, 4883 (1993).
[19] J. A. Oller, E. Oset, and J. R. Pelaez, Phys. Rev. Lett. **80**, 3452 (1998).
[20] J. A. Oller, E. Oset, and J. R. Pelaez, Phys. Rev. D **59**, 074001 (1999); **60**, 099906(E) (1999).
[21] J. A. Oller and E. Oset, Phys. Rev. D **60**, 074023 (1999).
[22] J. A. Oller and E. Oset, Nucl. Phys. **A620**, 438 (1997) [Erratum-*ibid*. **A652**, 407 (1997)].
[23] J. Gasser and H. Leutwyler, Nucl. Phys. **B250**, 517 (1985).
[24] E. Oset and M. J. Vicente Vacas, Nucl. Phys. **A678**, 424 (2000).
[25] J. Nieves and E. Ruiz Arriola, Nucl. Phys. **A679**, 57 (2000).
[26] J. Nieves and E. Ruiz Arriola, Phys. Lett. **B455**, 30 (1999).
[27] E. Oset, P. Fernandez de Cordoba, L. L. Salcedo, and R. Brockmann, Phys. Rep. **188**, 79 (1990).
[28] G. Chanfray and D. Davesne, Nucl. Phys. **A646**, 125 (1999).
[29] V. Bernard, N. Kaiser, and U. G. Meissner, Int. J. Mod. Phys. E **4**, 193 (1995).
[30] U. G. Meissner, J. A. Oller, and A. Wirzba, Ann. Phys. (NY) **297**, 27 (2002).
[31] H. C. Schroder *et al*., Phys. Lett. **B469**, 25 (1999).
[32] E. Oset and D. Strottman, Phys. Rev. Lett. **70**, 146 (1993).
[33] E. Oset, D. Strottman, H. Toki, and J. Navarro, Phys. Rev. C **48**, 2395 (1993).
[34] T. E. Ericson and W. Weise, *The International Series of Monographs on Physics* (Clarendon, Oxford, 1988), Vol. 74, p. 479.
[35] M. Herrmann, B. L. Friman, and W. Norenberg, Nucl. Phys. **A560**, 411 (1993).
[36] D. Cabrera, E. Oset, and M. J. Vicente Vacas, Nucl. Phys. **A705**, 90 (2002).
[37] R. A. Arndt, I. I. Strakovsky, R. L. Workman, and M. M. Pavan, Phys. Rev. C **52**, 2120 (1995).
[38] E. Oset and A. Ramos, Nucl. Phys. **A635**, 99 (1998).
[39] J. A. Oller and U. G. Meissner, Phys. Lett. **B500**, 263 (2001).
[40] V. Thorsson and A. Wirzba, Nucl. Phys. **A589**, 633 (1995).
[41] J. A. Oller and E. Oset, Phys. Rev. D **60**, 074023 (1999).
[42] G. Chanfray and D. Davesne, Nucl. Phys. **A646**, 125 (1999).
[43] M. Kirchbach and A. Wirzba, Nucl. Phys. **A604**, 395 (1996).
[44] N. Fettes and U. G. Meissner, Nucl. Phys. **A679**, 629 (2001).
[45] N. Fettes, U. G. Meissner, and S. Steininger, Nucl. Phys. **A640**, 199 (1998).
[46] E. Epelbaum, W. Gloeckle, and U. G. Meissner, Eur. Phys. J. A **19**, 125 (2004).
[47] M. J. Vicente Vacas and E. Oset, Sigma meson mass and width at finite density, arXiv:nucl-th/0204055.